NUMERICAL ANALYSIS OF MASONRY WALLS OUT-OF-PLANE LOADED

Gabriele Milani[1], Renato S. Olivito[2], Antonio Tralli[1], Francesca A. Zuccarello[2]

[1]University of Ferrara, Department of Engineering,
Via Saragat 1, 44100 Ferrara, Italy
[2]University of Calabria, Department of Structural Engineering
87036 Rende (CS), Italy

rs.olivito@unical.it (Renato S. Olivito)

Abstract

Masonry is a composite material constituted by the assemblage of bricks and mortar joints. It is commonly accepted that the mortar joints have a much lower strength than that of the bricks. As a consequence, there are preferential planes of weakness along which cracks propagate. This is particularly true in case of masonry panels out-of-plane loaded, where experimental evidences often show that failure lines follow the disposition of the bricks. Out-of-plane failures are mostly related to seismic and wind loads and the lack of out-of-plane strength is a primary cause of failure in different forms of masonry. In this paper, a heterogeneous approach for FE upper bound limit analyses of out-of-plane loaded masonry panels is presented. Under the assumption of associated plasticity for the constituent materials, mortar joints are reduced to interfaces with a Mohr-Coulomb failure criterion with tension cut-off and cap in compression, whereas bricks are supposed infinitely resistant. At each mortar interface, plastic dissipation can occur as a combination of out-of-plane shear, bending and torsional moment. In order to test the reliability of the model proposed, several experimental tests of dry-joint panels out-of-plane loaded have been carried out at the University of Calabria (Italy). Numerical results are compared with experimental evidences for three different series of walls at different values of the in-plane compressive vertical loads applied. The comparisons show that reliable predictions of both collapse loads and failure mechanisms can be obtained by means of the numerical procedure employed.

Keywords: Masonry, Heterogeneous Approach, Out-of-Plane Loads, FE limit analysis.

Presenting Author's biography

Renato Sante Olivito. He is Full Professor of Structural Engineering at the Department of Structural Engineering - Faculty of Engineering of the University of Calabria. His main research interests are Mechanics of Materials and Structures, with particular reference to Composite Materials and to non destructive techniques (ultrasonic and acoustic emission techniques) for the damage study and monitoring of civil structures. Further research interests concern: the study of the mechanical behaviour of masonry structures subjected to in-plane and out-of-plane loads; the study of durability of masonry and reinforced concrete structures reinforced by FRP materials.

ISBN 978-3-901608-32-2

1 Introduction

Masonry is one of the most ancient structural materials. The evaluation of the ultimate load bearing capacity of masonry elements is a key aspect for the design of new structures and the assessment of existing buildings.

Load bearing masonry walls are subjected simultaneously both to in-plane loads (self weight) and out-of-plane actions (earthquakes, wind, explosions, etc).

While masonry behavior subjected to in-plane actions has been widely investigated [1-2], relatively few papers devoted to the analysis of out-of-plane actions have been presented in the recent past in the technical literature [3-4-5]. Nevertheless, it is worth noting that the importance of the problem was stressed for the first time two centuries ago by Rondelet [6].

The recent earthquakes occurred in Italy confirmed that the lack of out-of-plane strength is a primary cause of failure in masonry structures [7-8] and that collapse is commonly caused by an inadequate interlocking between perpendicular walls. Moreover, laboratory tests conducted on brick masonry structures out-of-plane loaded [9-10-11-12] have shown that failure takes place along a well-defined pattern of lines, which usually follows the joints' disposition. As a consequence, the interfaces between bricks and mortar, have a much lower strength than that of the bricks, thus representing preferential planes of weakness along which cracks propagate.

Another important aspect that should be better investigated is the combined interaction of membrane and flexural loads. In fact, in-plane loads increase both the ultimate out-of-plane strength and the ductility of masonry, and bring additional complexity to the structural analysis.

From a numerical point of view, it has been shown [4-13] that classic limit analysis theorems can be profitably used for the prediction both of collapse loads and failure mechanisms of masonry structures in- and out-of-plane loaded. In this framework, different numerical models have been proposed in the past in the literature, based either on homogenization theory [4] or on a separate modeling of bricks and mortar joints [14].

In this paper, a heterogeneous approach is used in combination with limit analysis concepts for the analysis of both thin and thick masonry plates. A Finite Elements upper bound heterogeneous limit analysis model is presented based on a triangular discretization of the domain, where joints are reduced to interfaces with frictional behavior and limited tensile and compressive strength. Out-of-plane velocities interpolation is assumed to vary linear inside each element and possible jumps of velocities can occur at the interface between adjacent triangles. In this way, no dissipation is possible in continuum, whereas at each interface, plastic dissipation can occur as a combination of out-of-plane shear, bending and torsion. In this way the Reissner-Mindlin approach here proposed can be used for the analysis both of thick and thin plates, and it reduces to the well known Munro and Da Fonseca [15] triangular element (suitable for thin plates) when plastic dissipation is allowed only for bending moment. Moreover, the present approach allows, in principle, to take into account also bricks failure.

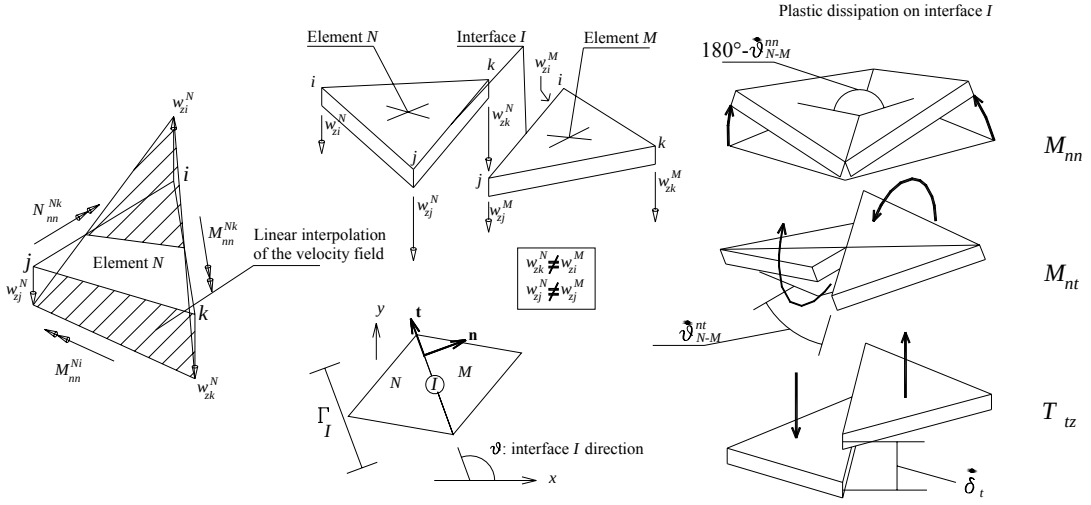

Fig. 1: Reissner-Mindlin FE kinematic limit analysis element. –a: field of velocities and discontinuity at each interface between adjacent triangles. –b: possible plastic dissipation at the interface due to bending moment, torsion and shear.

It is worth noting that the present heterogeneous out-of-plane approach, which takes into account out-of-plane failure due to a combined and simultaneous action of torsion, bending and shear, is new in the technical literature. For this reason, in order to assess the reliability of the numerical model proposed, a comparison with a number of experimental results, related to a set of tests conducted at University of Calabria (Italy) on three series of dry-joints masonry walls out-of-plane loaded [16-17], is made.

The good agreement between experimental data and numerical predictions shows the reliability of the numerical procedure presented [18].

2 Heterogeneous upper bound FE limit analysis of masonry walls out-of-plane loaded

In this section, a FE kinematic limit analysis model for the analysis of both thick and thin masonry walls is presented [18]. Reissner-Mindlin plate hypotheses are adopted.

The FE formulation is based on a triangular discretization of the wall, constituted by a regular assemblage of bricks disposed in running bond texture. Hence, each brick is meshed at least using 4 triangular elements in order to follow the actual disposition of the interfaces between adjacent bricks, i.e. dry-joints in the present case.

For each element E, one out-of-plane velocity unknown w_{zi}^{E} per node i is introduced, so that the velocity field is linear inside each element. Several nodes may share the same coordinate, being each node associated with only one element. In this way, at each interface between adjacent triangles, possible jumps of velocities can occur.

At each interface between adjacent elements M and N, both constant bending rotation rates $\dot{\vartheta}_{N-M}^{nn}$ and a torsional rotation rates $\dot{\vartheta}_{N-M}^{nt}$ can occur. Furthermore, an out-of-plane jump of velocities $\dot{\delta}_t$ which varies linearly along the interface is also considered. $\dot{\vartheta}_{N-M}^{nn}$, $\dot{\vartheta}_{N-M}^{nt}$ and $\dot{\delta}_t$ can be easily evaluated making use of the following linear relation between nodal velocities of adjacent elements M and N (see Fig. 1):

$$\begin{aligned}
&\dot{\boldsymbol{\theta}}_N = \mathbf{B}_N \mathbf{w}_z^N \\
&\dot{\vartheta}_{N-M}^{nt} = \frac{w_{zj}^M - w_{zi}^M}{\Gamma_I} - \frac{w_{zj}^N - w_{zk}^N}{\Gamma_I} \\
&\dot{\delta}_t = \left(w_{zj}^M - w_{zj}^N\right) + \frac{x_I}{\Gamma_I}\left[\left(w_{zi}^M - w_{zk}^N\right) - \left(w_{zj}^M - w_{zj}^N\right)\right] \qquad x_I \in [0 \quad \Gamma_I]
\end{aligned} \tag{1}$$

Where:

- $\mathbf{w}_z^N = \left[w_{zi}^N \quad w_{zj}^N \quad w_{zk}^N\right]^T$

- $$\mathbf{B}_N = \frac{1}{2A_N}\begin{bmatrix} \frac{b_i b_i + c_i c_i}{l_i} & \frac{b_i b_j + c_i c_j}{l_i} & \frac{b_i b_k + c_i c_k}{l_i} \\ \frac{b_j b_i + c_j c_i}{l_j} & \frac{b_j b_j + c_j c_j}{l_j} & \frac{b_j b_k + c_j c_k}{l_j} \\ \frac{b_k b_i + c_k c_i}{l_k} & \frac{b_k b_j + c_k c_j}{l_k} & \frac{b_k b_k + c_k c_k}{l_k} \end{bmatrix}$$

with $b_i = y_j - y_k$, $c_i = x_k - x_j$ and A_N is the element area;

- $\dot{\boldsymbol{\theta}}_N = \left[\dot{\vartheta}_i^N \quad \dot{\vartheta}_j^N \quad \dot{\vartheta}_k^N\right]^T$ are the side normal rotation rates, linked with $\dot{\vartheta}_{N-M}^{nn}$ by means of the linear equation $\dot{\vartheta}_{N-M}^{nn} = \dot{\vartheta}_i^N - \vartheta_i^M$;

- Γ_I is the interface length.

Power dissipated at each interface between adjacent triangles can be evaluated taking into account that three different elementary interface plastic dissipations can occur, related respectively to shear T_{tz}, bending moment M_{nn} and torsion M_{nt}.

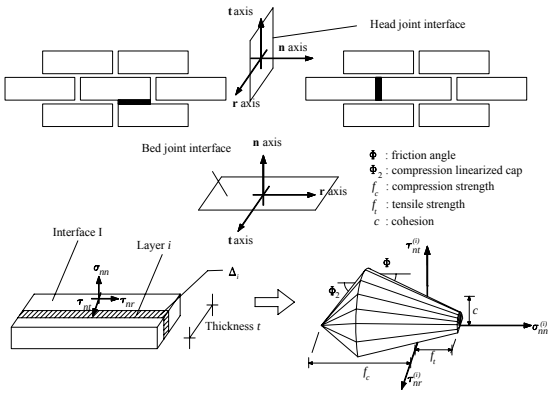

Fig. 2: Stresses acting on head and bed joint interfaces and failure surface adopted for joints.

A linearization of the interface failure surface $\Phi(T_{zt}, M_{nt}, M_{nn})$ is required. At this aim, in this paper a static approach is used to obtain a lower bound estimation of Φ. For each interface I, we assume that only normal stress σ_{nn} and two tangential stresses τ_{nt} and τ_{nr} along two assigned perpendicular directions act. The interface is subdivided along its thickness in a sufficiently large number of layers n_L of constant thickness $\Delta_i = t / n_L$, as shown in Fig. 2. In this way, three stress optimization unknowns per layer are introduced, being the stress vector $\boldsymbol{\sigma}^{(i)} = \left[\sigma_{nn}^{(i)} \quad \tau_{nt}^{(i)} \quad \tau_{nr}^{(i)}\right]^T$ kept constant along the i^{th} layer. In this way, the total

number of stress unknowns introduced is 3x n_L. Static admissibility is imposed in correspondence of each layer and involves, for the i^{th} layer, only $\sigma_{nn}^{(i)}$, $\tau_{nt}^{(i)}$ and $\tau_{nr}^{(i)}$ variables, once that a linearization of the failure surface $\phi = \phi\left(\boldsymbol{\sigma}^{(i)}\right)$ for each layer is provided.

In this work, a Mohr-Coulomb failure criterion combined with tension cut-off and cap in compression is adopted.

Within each layer i of the interface I, a piecewise linear approximation of the failure surface $\phi = \phi\left(\boldsymbol{\sigma}^{(i)}\right)$ is adopted, constituted by n_{lin} planes of equation $\mathbf{A}_k^{I\,T}\boldsymbol{\sigma}^{(i)} = c_k^I \quad 1 \le k \le n_{lin}$, where $\mathbf{A}_k^{I\,T}$ is a $1x3$ vector of coefficients and c_k^I is the right hand side of the k^{th} linearization plane.

In order to obtain a lower bound estimation of the interface failure surface, three equilibrium equations involving macroscopic actions T_{tz}, M_{nn} and M_{nt} and (integrated) internal stresses are further imposed, once that an optimization direction $\mathbf{n}_\lambda$ is a priori fixed in the $T_{tz} - M_{nn} - M_{nt}$ space.

In this way, the following linear optimization problem is obtained:

$$\begin{cases} \max(\lambda) \\ \text{subject to} \begin{cases} N = \int_\Gamma \sigma_{nn} dz \\ M_{nn} = \lambda \mathbf{n}_\lambda(1) = \int_\Gamma \sigma_{nn} z dz \\ M_{nt} = \lambda \mathbf{n}_\lambda(2) = \int_\Gamma \tau_{nt} z dz \\ T_{tz} = \lambda \mathbf{n}_\lambda(3) = \int_\Gamma \tau_{nr} dz \\ \mathbf{A}^{I\,T}\sigma^{(i)} \le \mathbf{c}^{(i)} \quad \forall i \in [1 \quad n_L] \end{cases} \end{cases} \qquad (2)$$

where λ is the limit load in the space $T_{tz} - M_{nn} - M_{nt}$, $\mathbf{n}_\lambda$ is the optimization direction. It is worth noting that for an accurate lower bound estimation of the failure surface several $\mathbf{n}_\lambda$ directions should be investigated and N is the membrane load perpendicular to the interface direction. It is worth underlining that, for the sake of simplicity N is kept constant. This implies that for bed joints we assume N equal to the applied in-plane vertical compressive load, whereas for head joints we assume N equal to zero.

Making use of Eq. (2) for several directions $\mathbf{n}_\lambda$, a linearization with m planes for the interface failure surface $\Phi(T_{zt}, M_{nt}, M_{nn})$ is easily obtained as $\mathbf{A}_I^{in}\hat{\mathbf{M}} \le \mathbf{C}_I^{in}$, where $\hat{\mathbf{M}} = [T_{zt} \quad M_{nt} \quad M_{nn}]$, $\mathbf{A}_I^{in}$ is a $mx3$ vector of coefficients and C_I^{in} is a vector of length m representing the right hand sides of the linearization planes.

Internal power dissipated at each interface is evaluated making use of the following expression:

$$P^I = \Gamma_I\left(M_{nn}\dot{\vartheta}_{nn} + M_{nt}\dot{\vartheta}_{nt}\right) + \frac{\Gamma_I}{2}\left(T_{zt}^{Ii}\dot{\delta}_{zt}^{Ii} + T_{zt}^{If}\dot{\delta}_{zt}^{If}\right) = \frac{\Gamma_I}{2}\sum_{q=1}^{m} C_{I,q}^{in}\left(\dot{\lambda}_{Ii}^{(q)} + \dot{\lambda}_{If}^{(q)}\right) \qquad (3)$$

where:

- $\dot{\lambda}_{Ii}^{(q)}$ and $\dot{\lambda}_{If}^{(q)}$ represent respectively the qth plastic multiplier rate of the initial (i) and final (f) point of the interface *I*, being the variation of plastic multiplier rates on interfaces linear;
- $\dot{\delta}_{zt}^{Ii}$ and $\dot{\delta}_{zt}^{If}$ are the jumps of velocities between elements N and M in correspondence of the initial (i) and final (f) point of the interface I, respectively.

It is worth noting that in Eq. (2) the well known normality rule, i.e. $\dot{\vartheta}_{nn} = \dot{\lambda}_I \partial\Phi / \partial M_{nn} = \sum_{q=1}^{m} \dot{\lambda}_I^{(q)} \mathbf{A}_I^{in}(q,1)$, has been used, which adds additional equality constraints for the optimization problem.

External power dissipated can be written as:

$$P^{ex} = \left(\mathbf{P}_0^T + \lambda \mathbf{P}_1^T\right)\mathbf{w} \qquad (4)$$

where $\mathbf{P}_0$ is the vector of equivalent lumped permanent loads; λ is the load multiplier, $\mathbf{P}_1$ is the vector of lumped variable loads and $\mathbf{w}$ is the vector of assembled nodal velocities.

As the amplitude of the failure mechanism is arbitrary, a further normalization condition in the form $\mathbf{P}_1^T\mathbf{w} = 1$ is usually introduced.

Hence, the external power becomes linear in $\mathbf{w}$ and λ:

$$P^{ex} = \mathbf{P}_0^T\mathbf{w} + \lambda \qquad (5)$$

After elementary assemblage operations, the following optimization problem is obtained:

$$\begin{cases} \min\left\{\sum_{i=1}^{n^I} P^I - \mathbf{P}_0^T\mathbf{w}\right\} \\ \text{such that} \begin{cases} \mathbf{A}^{eq}\mathbf{U} = \mathbf{A}^{eq}\left[\mathbf{w} \quad \tilde{\dot{\boldsymbol{\theta}}}_{nn} \quad \tilde{\dot{\boldsymbol{\theta}}}_{nt} \quad \tilde{\dot{\boldsymbol{\delta}}}_{zt} \quad \dot{\boldsymbol{\lambda}}^{I,ass}\right] = \mathbf{b}^{eq} \\ \dot{\boldsymbol{\lambda}}^{I,ass} \ge \mathbf{0} \end{cases} \end{cases} \qquad (6)$$

where $\mathbf{C}_E^T$ and $\mathbf{C}_I^T$ are the (assembled) right-hand sides of the inequalities which determine the linearized failure surface of the homogenised material respectively in continuum and in the interfaces and

$\mathbf{U} = \left[\mathbf{w} \quad \tilde{\dot{\boldsymbol{\theta}}}_{nn} \quad \tilde{\dot{\boldsymbol{\theta}}}_{nt} \quad \tilde{\dot{\boldsymbol{\delta}}}_{zt} \quad \dot{\boldsymbol{\lambda}}^{I,ass} \right]$ is the vector of global unknowns, which collects the vector of assembled nodal velocities ($\mathbf{w}$), the vector of assembled bending interface rotation rates ($\tilde{\dot{\boldsymbol{\theta}}}_{nn}$), the vector of assembled torsion interface rotation rates ($\tilde{\dot{\boldsymbol{\theta}}}_{nt}$), the vector of assembled jump of velocities on interfaces ($\tilde{\dot{\boldsymbol{\delta}}}_{zt}$) and the vector of assembled interface plastic multiplier rates ($\dot{\boldsymbol{\lambda}}^{I,ass}$).

It is worth noting that in Eq. (2), $\mathbf{A}^{eq}$ is the overall constraints matrix and collects velocity and rotation boundary conditions, relations between rotation rates, velocity jumps on interfaces and elements velocities and constraints for plastic flow in velocity discontinuities. However, refer to [18] for a deeper development of the model implementation.

3 Numerical model validation

In order to assess the reliability of the numerical model proposed, in this section a comparison with a number of experimental results, related to a set of tests [16-17-18] conducted at University of Calabria (Italy), is reported. As shown in [16-17], three different series of dry-joint masonry panels were tested. Each wall, of dimension 100x100cm^2 was arranged in running bond texture using 1:3 scale bricks, without mortar. In-scale models were used in order to reproduce in a simple way a 300x300cm^2 masonry wall, trying to represent the real behavior of a wall inside a real building (Fig. 3).

For each series, three sub-series (which differ only for the constant vertical compressive load, equal to 7, 10 and 13 kN respectively) were loaded until failure by means of the application of a concentrated out-of-plane force, perpendicularly to the frontal surface of the panel. For each sub-series, at least three panels were experimentally tested, nevertheless, for the sake of conciseness, load-displacement curves relative to the investigated points are reported only for one panel of each sub-series. See [16-17-18] for a better description of the experimental program, materials adopted and experimental procedure.

Fig. 3: Steel frame, instrumentation and tested panel.

In the first series (Series A), the lower edge and one of the lateral sides of the panels were clamped and constrained to a stiff steel frame, whereas the remaining two sides were free both to rotate and move. The out-of-plane force was applied in correspondence to the right top edge of the model.

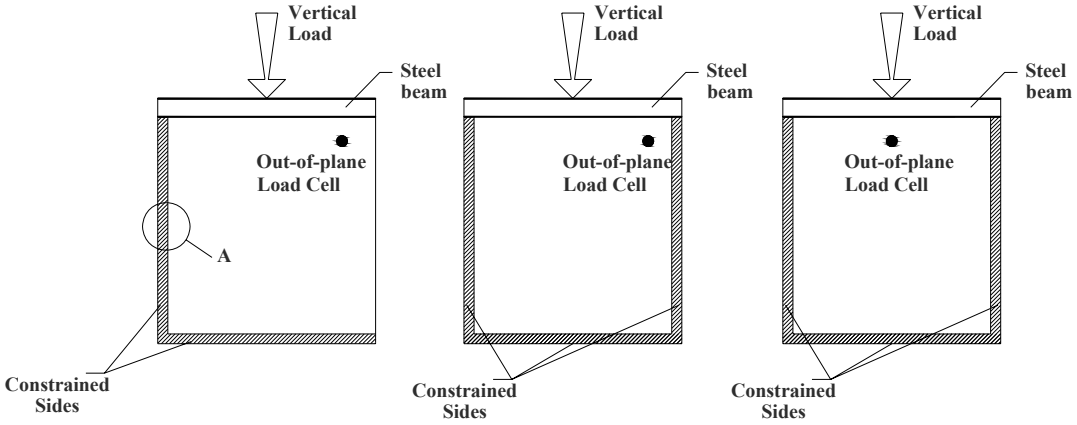

Fig. 4: Loading and constraint conditions. –a: series A. –b: series B. –c: series C.

In the second series (Series B), three sides were clamped, whereas the top surface was free to move. Also in this case, the horizontal force was applied eccentrically at the top of the specimens. The third series (Series C) differs from Series B only for the point of application of the out-of-plane load, placed in this case at the top-center of the specimens (Fig. 4).

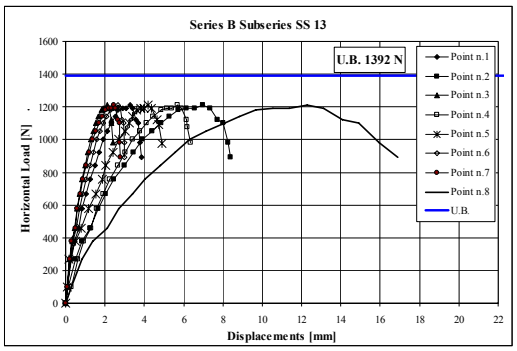

-a

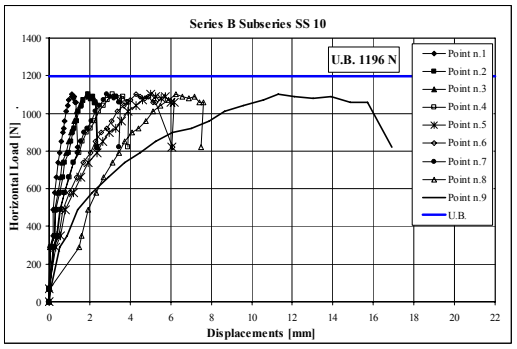

-b

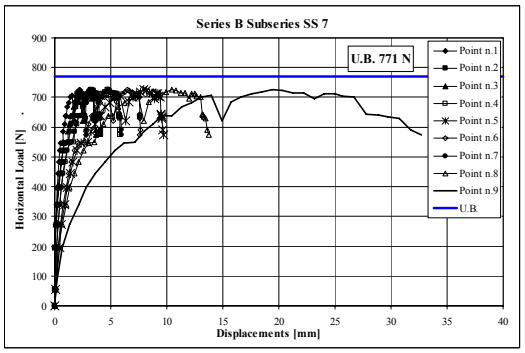

-c

Fig. 5: -a: Load-displacement curves: series B-SS 13. –b: Load-displacement curves: series B-SS 10. –c: Load-displacement curves: series B-SS 7.

During the tests, load-displacement curves were obtained registering displacement values by means of centesimal mechanically operated dial gauges and linear inductive displacement transducers, placed in different points of the specimens. Moreover, a 3D representation of the deformed shape at collapse has been post-processed from experimental data acquired. Such a procedure made a comparison between numerical and experimental failure mechanisms possible.

Here, for the sake of conciseness, only the experimental results relative to series B tests are reported. In particular, Fig. 5 shows a comparison between experimental load-displacement curves and numerical collapse load obtained applying the upper bound procedure proposed. Furthermore, Fig. 6 and Fig. 7 show a comparison between experimental and numerical deformed shapes at collapse.

For Series B SS 13 the horizontal collapse load reached was approximately equal to 1200 N, for Series B SS 10 approximately 1100 N, for Series B SS 7 approximately 700 N (Fig. 5).

The area involved by the cracks is restricted to the zone near the point of application of the horizontal device, because of the constraint conditions (Figs. 6 and 7).

The reliability of the numerical results should be noted. In particular, the numerical deformed shape at collapse reproduces very well the out-of-plane sliding of the bricks in correspondence to the point of application of the load, see Fig. 7.

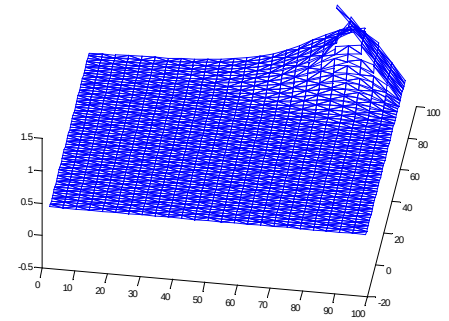

-a

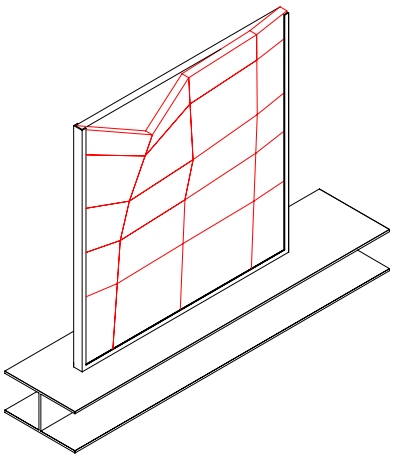

-b

Fig. 6: Comparison between numerical (-a) and experimental (-b) collapse mechanisms, series B.

For the numerical analysis, a FE model with 1375 nodes and 2592 elements has been used. A linearization with 44 planes for each interface between adjacent triangles was implemented in the FE upper bound limit analysis code, assuming for mortar joints interfaces a Mohr-Coulomb failure criterion with friction angle equal to 30° and cohesion equal to 0.01 N/mm^2. Such values are derived from experimental data collected on dry-joints.

Finally, in Fig. 8, a comparison between experimental and numerical deformed shapes at collapse for series C walls is shown. It can be noticed that the failure mechanism is similar to that obtained for series B, except for the different position of the plastic hinges.

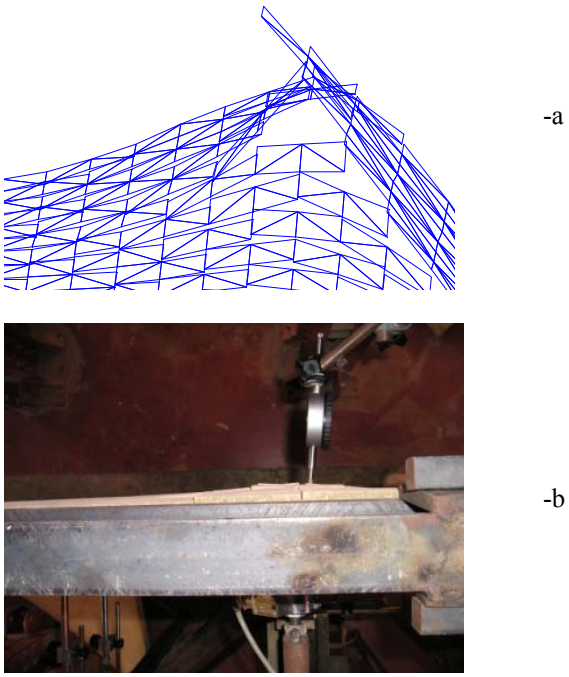

-a

-b

Fig. 7: Series B. Detail of failure mechanism in correspondence of the point of application of the load (-a) numerical (-b) experimental.

4 Conclusions

In this paper, a heterogeneous upper bound FE model for the limit analysis of out-of-plane loaded masonry walls has been presented. Numerical results for three different series of masonry panels out-of-plane loaded have been compared with experimental data collected at the University of Calabria. Experimentation has been carried out with the aim of studying the collapse mechanisms of dry-joint masonry subjected to out-of-plane actions (e.g. wind, earthquake, explosions).

For all the series analyzed, FE limit analysis results fit well experimental data, for what concerns both failure mechanisms and ultimate loads.

The comparison between experimental data and numerical limit analysis results underlines that reliable predictions of both collapse loads and failure mechanisms can be obtained with the numerical model presented.

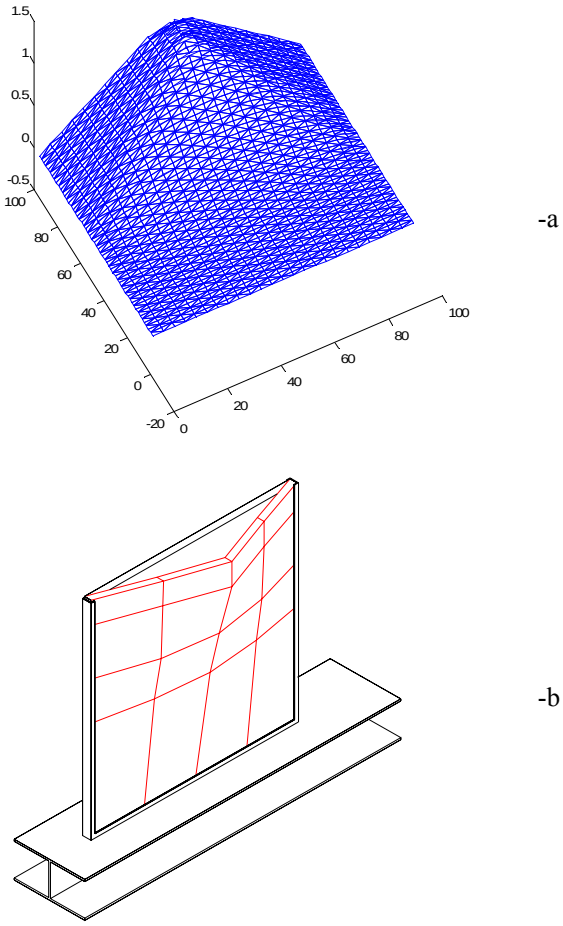

-a

-b

Fig. 8: Comparison between numerical (-a) and experimental (-b) collapse mechanisms, series C.

5 References

[1] Cecchi A., Milani G., Tralli A. (2004). In-plane loaded CFRP reinforced masonry walls: mechanical characteristics by homogenisation procedures. Composites Science and Technology, 64: 2097-2112.

[2] Anthoine A. (1995). Derivation of the in-plane elastic characteristics of masonry through homogenisation theory. Int. J. Solids Structures, 32: 137-163.

[3] Lourenço PB (2000) Anisotropic softening model for masonry plates and shells. ASCE Jour. Struct. Eng. 126(9): 1008–1016.

[4] Milani G, Lourenço PB, Tralli A (2006) Homogenization approach for the limit analysis of out-of-plane loaded masonry walls. ASCE Jour. Struct. Eng. 132(10): 1650-1663.

[5] Cecchi A, Milani G, Tralli A (2006) A Reissner-Mindlin limit analysis model for out-of-plane loaded running bond masonry walls. International Journal of Solids and Structures 44(5): 1438-1460.

[6] Rondelet JB (1802) Traité théorique et pratique de l'art du batir. Paris.

[7] Spence R, Coburn A (1992) Strengthening building of stone masonry to resist earthquakes. Meccanica 27: 213–221.

[8] Borri A, Avorio A, Cangi G (2001) Guildelines for seismic retroffiting of ancient masonry buildings. Rivista italiana di geotecnica 4: 112-121.

[9] Chee Liang NG (1996) Experimental and theoretical investigation of the behavior of brickwork cladding panel subjected to lateral loading. PhD Thesis, University of Edinburgh, Scotland.

[10] Guggisberg R, Thurlimann B (1988) Failure criterion for laterally loaded masonry walls: Experimental investigations. In Proc: 8th Int. Brick/Block Masonry Conf., Ireland.

[11] Van Der Pluijm, R (1999) Out-of-plane bending of masonry. Behaviour and strength. PhD Thesis, Eindhoven University of Technology, The Nederlands.

[12] West HWH, Hodgkinson HR, Haseltine BA (1977) The resistance of brickwork to lateral loading. The Structural Engineer 10 (55).

[13] Milani G, Lourenço PB, Tralli A (2006) Homogenised limit analysis of masonry walls. Part II: structural examples. Computers and Structures 84, 181-195.

[14] Sutcliffe DJ, Yu HS, Page AW (2001) Lower bound limit analysis of unreinforced masonry shear walls. Computers and Structures 79: 1295-1312.

[15] Munro J, Da Fonseca AMA (1978) Yield-line method by finite elements and linear programming. ASCE Jour. Struct. Eng. 56B: 37-44.

[16] Olivito RS, Zuccarello FA (2006). Indagine sperimentale sul comportamento meccanico di pareti murarie caricate fuori dal piano [Experimental analysis on the mechanical behavior of masonry walls out-of-plane loaded]. In Proc: XXXV National Conference AIAS, Ancona, Italy.

[17] Zuccarello F.A. (2006). Analisi teorico-sperimentale di pareti murarie caricate fuori dal piano [Theoretical and experimental analysis of masonry panels out-of-plane loaded]. PhD Thesis, Department of Structural Engineering, University of Calabria, Novembre 2006.

[18] Milani G., Zuccarello F.A., Olivito R.S., Tralli A. (2007). Heterogeneous upper-bound finite element limit analysis of masonry walls out-of-plane loaded. In Press on Computational Mechanics, ISSN 0178-7675.

